Variable Conformation and Dynamics of Calmodulin Complexed with Peptides Derived from the Autoinhibitory Domains of Target Proteins†

Yihong Yao and Thomas C. Squier*

Department of Biochemistry, University of Kansas, Lawrence, Kansas 66045-2106

Received January 30, 1996; Revised Manuscript Received April 5, 1996⊗

ABSTRACT: Calcium-saturated calmodulin (CaM) can bind and activate many target proteins through the direct association with the respective autoinhibitory domains. The CaM binding sequences within the autoinhibitory domains of these proteins have little sequence homology, and the mechanisms associated with CaM's ability to recognize and productively bind with these variable sequences is unclear. Common structural features of CaM bound to five peptides that are homologous to the autoinhibitory domains of smooth muscle myosin light chain kinase, CaM-dependent protein kinase IIα, the plasma membrane Ca-ATPase, a MARCKS homolog, and glycogen phosphorylase kinase were assessed using frequency-domain fluorescence spectroscopy. In addition, the structural features of CaM complexed with the peptide melittin was also considered. We observe similar decreases in the average fluorescence lifetime and similar increases in the solvent accessibility of *N*-(1-pyrenyl)maleimide (PM) bound at Cys_{27} in calcium binding loop I in the amino terminal domain of CaM upon association with all six target peptides. Likewise, using fluorescence resonance energy transfer to measure the spatial separation between the opposing globular domains in CaM, we observe a similar spatial separation between the opposing globular domains of CaM bound to all six peptides. This indicates that CaM undergoes comparable structural changes upon association with all six target peptides. However, there are significant differences in the observed lifetime, solvent accessibility, correlation time associated with the segmental rotational motion of PM-CaM, and in the spatial separation between the opposing globular domains in CaM upon association with the individual target peptides, which indicates that CaM adopts a different tertiary structure that is dependent on the structural features of the bound target peptide. The correlation times associated with the overall hydrodynamic properties of CaM complexed with all six peptides are nearly identical ($\phi_2 \approx 10.6 \pm 0.4$ ns) and are consistent with the known dimensions of CaM complexed to a peptide homologous to the CaM binding sequence of CaM-dependent protein kinase IIα. Therefore, while these results are consistent with a common binding mechanism between CaM and all six target peptides, they indicate that the binding domains of CaM adopt different tertiary structures that allow them to bind with the variable sequences found in the autoinhibitory domains of target proteins with high affinity.

Calmodulin (CaM)[1] is an intracellular calcium sensor that is involved in the coordinate regulation of the activity of a large variety of proteins associated with intracellular signaling and metabolism [reviewed by James et al. (1995)]. The crystal structure of the calcium-liganded form of CaM contains two structurally homologous globular domains connected by a seven-turn α-helix (Babu et al., 1985, 1988). The central helix is conformationally disordered (Babu et al., 1988), resulting in considerable heterogeneity with respect to the spatial separation between the opposing globular domains in both apo- and calcium-saturated CaM (Barbato et al., 1992; Yao et al., 1994; Tjandra et al., 1995), and has been proposed to be important with respect to the ability of CaM to associate with a range of target proteins whose autoinhibitory sequences have both little sequence similarity and in which the spacing of key hydrophobic residues in the primary sequence of target peptides thought to be associated with CaM binding is highly variable [Ikura et al., 1992; Meador et al., 1993; reviewed by Crivici and Ikura (1995)].

Understanding the mechanisms relating to CaM's ability to recognize and activate a range of diverse target proteins with variable binding sequences is critical to a quantitative understanding of calcium signaling in cellular metabolism.

† Supported by the American Heart Association Grant 1697 and the National Institutes of Health Grants GM46837 and AG12993.

* Correspondence should be addressed to this author. Tel: (913) 864-4008. FAX: (913) 864-5321. E-mail: TCSQUIER@KUHUB.CC.UKANS.EDU.

⊗ Abstract published in *Advance ACS Abstracts,* May 15, 1996.

[1] Abbreviations: CaM, calmodulin; C25W, a peptide homologous to the calmodulin binding sequence on the autoinhibitory domain of the plasma membrane Ca-ATPase whose sequence is QILWFRGLNRIQTQIRVVNAFRSSC (a cysteine at the carboxyl terminal provides an attachment sites for fluorophores on the peptide); CAMKII20, a peptide homologous to the calmodulin binding sequence on the autoinhibitory domain of the brain calmodulin dependent protein kinase IIα, whose sequence is LKKPNARRKLKGAILTTMLA; CAPS, 3-(cyclohexylamino)propanesulfonic acid; DTT, dithiothreitol; EGTA, ethylene glycol bis(β-aminoethyl ether)-*N*,*N*,*N*′,*N*′-tetraacetic acid; F52, a peptide homologous to the calmodulin binding sequence on the autoinhibitory sequence of MARCKS homolog whose sequence is KKKKKFSFKKPFKLSGLSFKRNRK; FRET, fluorescence resonance energy transfer; GnHCl, guanidinium hydrochloride; HEPES, *N*-[2-hydroxyethyl]piperazine-*N*′-[2-ethanesulfonic acid]; HPLC, high-performance liquid chromatography; PHK5, a peptide homologous to the calmodulin binding sequence on the autoinhibitory sequence of glycogen phosphorylase kinase whose sequence is LRRLIDAYAFRIYGHWVKKGQQQNRG; PM, *N*-(1-pyrenyl)maleimide; RS20, a peptide homologous to the calmodulin binding sequence on the autoinhibitory sequence of the smooth muscle myosin light chain kinase whose sequence is ARRKWQKTGHAVRAIGRLSS; TEMPAMINE, 4-amino-2,2,6,6-tetramethyl-1-piperidinyloxyl; TNM, tetranitromethane.

S0006-2960(96)00229-2 CCC: $12.00

It is now clear that the CaM binding domains of a variety of target peptides have a propensity to form basic amphipathic α-helices [reviewed by Erickson-Vitanen and DeGrado (1987) and Trewhella (1992); O'Neil & Degrado, 1990]. Two high-resolution crystal structures of CaM in association with target peptides are currently available (i.e., peptides derived from the autoinhibitory domains of smooth muscle myosin light chain kinase and CaM-dependent protein kinase IIα; Meador et al., 1992, 1993), and the general features of the complex are consistent with the average solution structure of CaM complexed with a 26 amino acid peptide homologous to the CaM binding domain of skeletal muscle myosin light chain kinase as determined by high-field NMR data (Ikura et al., 1992). In all cases the α-helical target peptide is located in a hydrophobic channel that passes through the center of the ellipsoid at an angle of ~45° relative to the long axis of the CaM:peptide complex (Ikura et al., 1992; Meador et al., 1992, 1993). A comparison of the two crystal structures demonstrates that, while critical groups on the target peptides involved in the binding interaction with CaM have a variable spacing within the primary structure of the peptide, there is a similar spatial separation between specific amino acids in CaM within the tertiary structures of CaM complexed to both RS20 and CaMKII (Meador et al., 1993). This suggests a degree of flexibility with respect to the peptide binding sites within the tertiary structure of CaM and suggests that CaM can bind a range of target proteins without the need to alter the spatial arrangement of the opposing globular domains (Afshar et al., 1994). From these studies it is unclear what role the reported flexibility of the central helix may play in promoting the association of CaM with the variable binding sites found on target proteins. Measurements relating to the hydrodynamic properties of CaM indicate that the two opposing globular domains in calcium-activated CaM are structurally coupled (Small & Anderson, 1988; Török et al., 1992; Yao et al., 1994), and small-angle X-ray and neutron diffraction measurements of CaM bound to target peptides indicate that many of the general features associated with the binding of the opposing globular domains in CaM to recognition sites on target proteins are conserved [reviewed by Trewhella (1992)]. This suggests that the structural properties of the central helix may be critical in defining the optimal spatial relationship between the opposing globular domains in CaM for the rapid and efficient activation of target proteins. The conformational flexibility observed in the central helix may facilitate the optimal interaction between CaM and target peptides, and may allow CaM to rapidly associate with autoinhibitory domains in target proteins in which there is a variable separation between important hydrophobic amino acids associated with CaM binding. The presence of multiple binding pockets within CaM is consistent with observations involving the association of CaM with target sequences in altered conformations (Afshar et al., 1994). It is, however, unclear if the spatial relationship between the opposing globular domains of calcium-saturated CaM bound to a range of target peptides is critical to the ability of CaM to bind to and activate target proteins on the millisecond time scale.

In order to probe the general mechanisms relating to how calcium-activated CaM interacts with target peptides that have little sequence homology, we have used frequency-domain fluorescence spectroscopy to assess the structure of wheat germ CaM bound to six target peptides. We have covalently attached *N*-(1-pyrenyl)maleimide (PM) to the single Cys_{27} in calcium binding site I, which permits the identification of conformational and structural changes associated with the amino terminal domain of wheat germ CaM upon binding to target peptides (Figure 1). Lifetime-resolved fluorescence resonance energy transfer (FRET) between PM and $nitrotyrosine_{139}$ located in calcium binding loop IV provide information regarding the average separation and distance heterogeneity between fluorophores associated with the opposing globular domains of CaM upon interacting with target peptides. Complementary measurments of fluorescence quenching and anisotropy permit us to compare the local and global conformational changes of CaM upon binding to all six target peptides.

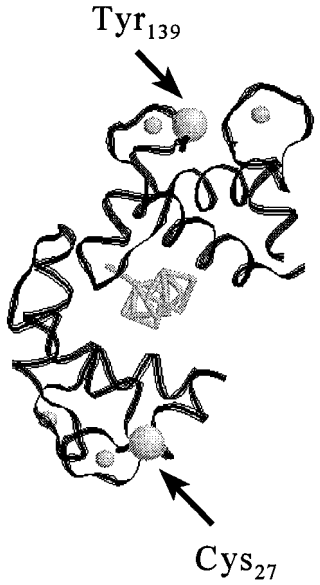

FIGURE 1: Positions of donor and acceptor chromophores within calmodulin. The relative positions of Cys27 (binding site for PM) and Tyr139 (which is nitrated to form an energy-transfer acceptor) are highlighted in the ribbon drawing of the backbone fold of the calcium saturated form of CaM bound to a target peptide from calmodulin-dependent protein kinase IIα. The coordinates are taken from the Brookhaven Protein Data Bank file 1 cdm.pdb (Meador et al., 1993), and the ribbon drawing was created using the shareware program RASMOL. The small filled circles represent calcium ligands.

EXPERIMENTAL PROCEDURES

Materials. *N*-1-(Pyrenyl)maleimide (PM) and 1-(2-2(5-carboxyoxazol-2-yl)-6-aminobenzofuran-5-yl-2-(2′-amino-5′-methylphenoxy)ethane-*N*,*N*,*N*′,*N*′-tetraacetic acid) (FURA-2) were obtained from Molecular Probes, Inc. (Junction City, OR). Tetranitromethane (TNM) was obtained from Aldrich (Milwaukee, WI). CAMKII20 (LKKPNARRKLKGAIL-TTMLA), a calmodulin binding domain derived from calmodulin-dependent protein kinase IIα was purchased from Signal Transduction Inc. (San Diego, CA). All other reagent chemicals were the purest grade commercially available. CaM was purified from wheat germ using the procedure outlined by Strasburg et al. (1988), and purity was assessed by both SDS−PAGE and HPLC. Purified wheat germ CaM was stored at −70 °C. The C25W peptide (QILWFRGLN-RIQTQIRVVNAFRSSC) was synthesized by the Kansas State University Biotechnology Microchemical Core Facility. The F52 peptide (KKKKKFSFKKPFKLSGLSFKRNRK), melittin peptide (GIGAVLKVLTTGLPALISWIKRKRQQ),

and RS20 peptide (ARRKWQKTGHAVRAIGRLSS) were generous gifts from J. David Johnson (Ohio State University). The PHK5 peptide (LRRLIDAYAFRIYGHWVKKGQQQN-RG) was a generous gift from Robert Steiner (University of Maryland).

Specific Derivitization of CaM. The specific nitration of the single Tyr_{139} in wheat germ CaM and the chemical modification of Cys_{27} with PM was carried out as previously described (Yao et al., 1994). Prior to chemical derivitization, CaM was first dissolved in 6 M GnHCl, 25 mM HEPES (pH 7.5), 50 mM DTT and 1 mM EDTA buffer and incubated at room temperature for 2 h in order to eliminate intermolecular cross-linking. DTT was removed either by exhaustive dialysis against deionized water or by using size-exclusion chromatography (i.e., a 1.6 × 23 cm Sephadex G-25 column), and the desalted CaM was subsequently lyophilized. The concentration of wheat germ CaM was determined using the micro BCA assay (Pierce), using a stock solution of desalted bovine CaM whose concentration was determined using the published extinction coefficient for bovine CaM as a standard ($\epsilon_{277} = 3029\ M^{-1}\ cm^{-1}$; Strasburg et al., 1988). Derivitized CaM was stable at −70 °C for at least 2 months, as evidenced by the ability to activate the erythrocyte Ca-ATPase and fluorescence measurements relating to protein structural changes (Yao et al., 1994). The extent of nitration was measured in 6 M GnHCl, 1 mM EDTA, and 50 mM CAPS (pH 10) using the molar extinction coefficient $\epsilon_{428} = 4200\ M^{-1}\ cm^{-1}$ for nitrotyrosine (Richman & Klee, 1978) and corresponded to 0.95 ± 0.05 mol of nitrotyrosine per mol of CaM. The extent of modification with PM was determined using the molar extinction coefficient of PM ($\epsilon_{343} = 36\,000\ M^{-1}\ cm^{-1}$) and corresponded to 0.95 ± 0.06 mol of pyrene maleimide per mol of CaM.

Concentration of Target Peptides. The concentration of C25W was determined using the published extinction coefficient (i.e., $\epsilon_{280} = 5600\ M^{-1}\ cm^{-1}$; Chapman et al., 1992). The peptide concentration of CaMKII20 was determined by amino acid composition analysis by the supplier (Signal Transduction Inc., San Diego, CA). PHK5 was a kind gift from Dr. Steiner (University of Maryland), and the concentration of PHK5 was computed assuming the molar extinction coefficient at 280 nm to be equal to the summed extinction coefficients of the aromatic amino acids present in the peptide (Juminaga et al., 1994). The F52, RS20, and melittin peptides were kind gifts from Dr. J. David Johnson (Ohio State University), who supplied their respective concentrations based on a determination from absorption spectrophotometry in conjunction with amino acid composition analysis (Graff et al., 1989).

Determination of Binding Affinities between CaM and Target Peptides. Peptide binding affinities to CaM were assessed using the associated decrease in the steady-state fluorescence intensity of PM-CaM upon peptide binding, as described in Results. This analysis assumes that there is a linear relationship between the decrease in the fluorescence signal and peptide binding and that one mole of peptide binds one mole of CaM, as previously determined [reviewed by Crivici and Ikura (1995)], implying that

$$[\text{Peptide}]_{\text{bound}} = \left[\frac{|(F - F_0)|}{|(F_{\max} - F_0)|}\right] \times [\text{CaM}]_{\text{total}} \qquad (1)$$

where F_0 is the initial fluorescence, $F_{\max}$ is the fluorescence observed in the presence of saturating concentrations of peptide, and F is the observed fluorescence at a particular peptide concentration. $[\text{CaM}]_{\text{total}}$ is the total concentration of CaM in solution, and $[\text{Peptide}]_{\text{bound}}$ is the concentration of peptide that is associated with CaM. Knowing $[\text{Peptide}]_{\text{bound}}$ it is possible to calculate the concentration of peptide free in solution (i.e., $[\text{Peptide}]_{\text{free}}$), where

$$[\text{Peptide}]_{\text{free}} = [\text{Peptide}]_{\text{total}} - [\text{Peptide}]_{\text{bound}} \qquad (2)$$

Therefore, if one assumes a homogeneous population of independent peptide binding sites on CaM one can calculate the apparent association constant (K_a) assuming a simple binding isotherm (Pedigo & Shea, 1995), where

$$[\text{Peptide}]_{\text{bound}} = \left(\frac{K_a[\text{Peptide}]_{\text{free}}}{1 + K_a[\text{Peptide}]_{\text{free}}}\right) \times \text{Span} + \text{Minimum} \qquad (3)$$

Span is related to the extent of peptide binding offset by a minimum value. Experimental data were fitted using the Levenberg−Marquardt algorithm contained in the program ORIGIN (Microcal Software, Inc., Northampton, MA).

Spectroscopic Measurements. Fluorescence lifetime and anisotropy measurements were performed using an ISS K2 frequency-domain fluorimeter, whose design has previously been described in detail (Gratton & Limkeman, 1983). This instrument is equipped with a Marconi signal generator (2022A & C) and ENI broad-band amplifiers (325LA and 403LA) which operate in conjunction with a Pockels cell to obtain intensity-modulated light at 351 nm from a CW argon ion laser (Coherent Innova 400, Santa Clara, CA).

Fluorescence emission spectra and quenching experiments were performed using an ISS K2 fluorimeter in the ratio mode. TEMPAMINE was added in microliter increments to 2 mL of 1.2 μM PM-CaM in 0.1 M KCl, 1 mM $MgCl_2$, 0.10 M HEPES (pH 7.5), and 0.1 mM $CaCl_2$. Excitation was at 351 nm. Fluorescence emission was collected using a Schott GG400 long-pass filter. Analysis of the collisional quenching was carried out essentially as described by Lehrer and Leavis (1978), and the effect of the quencher on the steady-state fluorescence of a sample is described by the Stern−Volmer equation

$$\frac{F_0}{F} = 1 + K_{sv}[\text{Q}] = \frac{\bar{\tau}_0}{\bar{\tau}} \qquad (4)$$

where F_0 and F are the fluorescence intensity in the absence and presence of the quencher, $\bar{\tau}_0$ and $\bar{\tau}$ are the average fluorescence lifetimes in the absence and presence of the quencher, K_{sv} is the Stern−Volmer quenching constant and is the slope of the plot F_0/F versus quencher concentration.

From K_{sv} and the average fluorescence lifetime of the fluorophore ($\bar{\tau}$), one can determine the bimolecular collisional frequency k_q, which is directly related to the solvent exposure of the fluorophores and is related to K_{sv} and $\bar{\tau}$ by the following equation:

$$k_q = \frac{K_{sv}}{\bar{\tau}} \qquad (5)$$

where $\bar{\tau}$ represents the amplitude weighted average lifetime (see below).

Decays of Fluorescence Intensities. The time-dependent decay $I(t)$ of any fluorophore can always be described as a sum of exponentials,

$$I(t) = \sum_{i=1}^{n} \alpha_i \, e^{(-t/\tau_i)} \tag{6}$$

where α_i are the pre-exponential factors, τ_i are the excited state decay times, and n is the number of exponential components required to describe the decay. The intensity decay law is obtained from the frequency-response of the amplitude-modulated light and is characterized by the frequency (ω) dependent values of the phase-shift (ϕ_ω) and the extent of demodulation (m_ω). The parameters describing the decay law are compared with the calculated values ($\Phi_{c\omega}$ and $m_{c\omega}$) from an assumed decay law, and the parameters chosen are those that minimize the squared deviation. Explicit expressions have been provided that permit the ready calculation of α_i and τ_i (Weber, 1981). The parameter values are determined by minimizing the χ_R^2 (the F statistic) which serves as a goodness-of-fit parameter that provides a quantitative comparison of the adequacy of different assumed models (Lakowicz & Gryczynski, 1991). Data are fitted using the method of nonlinear least-squares to a sum of exponential decays (Bevington, 1969). Subsequent to the measurement of the intensity decay, one typically calculates the average lifetime, $\bar{\tau}$, which is weighted by the amplitudes associated with each of the pre-exponential terms, where

$$\bar{\tau} \equiv \sum_i \alpha_i \tau_i \tag{7}$$

and $\bar{\tau}$ is directly related to the average time the fluorophore is in the excited state, and the amplitude weighing implies a direct relationship between $\bar{\tau}$ and the quantum yield of the fluorophore (Luedtke et al., 1981). Alternatively, for the case of fluorescence resonance energy transfer measurements more realistic physical models were used involving a distribution of distances (see below), as previously described (Haas et al., 1978; Lakowicz et al., 1988; Yao et al., 1994).

Calculation of Molecular Distances using FRET. Utilizing FRET to measure the distance between any fluorophore (donor; D) and a suitable acceptor (A) chromophore, one can measure distances in the 10−100 Å range, and directly recover structural information concerning biological macromolecules (Stryer, 1978). The efficiency of energy transfer, E, and the apparent donor-acceptor distance, r_{app}, are calculated from the Förster equations (Fairclough & Cantor, 1978), where

$$E = 1 - \frac{F_{da}}{F_d} = 1 - \frac{\bar{\tau}_{da}}{\bar{\tau}_d} \quad \text{and} \quad E = \frac{R_o^{\,6}}{R_o^{\,6} + r_{app}^{\,6}} \tag{8}$$

and F_{da} and F_d are the steady-state fluorescence intensities in the presence and absence of the acceptor (nitrotyrosine), $\bar{\tau}_{da}$ and $\bar{\tau}_d$ are the average fluorescence lifetime (see eq 7) of the donor in the presence and absence of the acceptor (nitrotyrosine), and R_o is the Förster critical distance that defines the distance for a given donor−acceptor pair where the efficiency of resonance energy transfer is 50%. $\bar{\tau}_{da}$ and $\bar{\tau}_d$ are determined from frequency-domain measurements relating to the fluorescence intensity decay of PM-CaM in the presence and absence of nitrotyrosine (see above). R_o (in cm) is given by

$$R_o = 9.79 \times 10^{-5} \, (n^{-4} \kappa^2 \phi_d J)^{1/6} \tag{9}$$

where n is the refractive index, κ^2 is the orientation factor, J is overlap integral, and ϕ_d is the quantum yield of the donor in the absence of acceptor. In our experiments, n is estimated to be 1.40 (Fairclough & Cantor, 1978); κ^2 is assumed to be $^2/_3$, which assumes that donor and acceptor chromophores undergo rapid isotropic rotational motion relative to the lifetime of the donor (see below); ϕ_d is determined by numerical integration of the fluorescence emission spectrum of PM-CaM, using quinine sulfate as a standard, which has a quantum yield of 0.70 in 0.1 N H_2SO_4 (Scott et al., 1970); and J is calculated by numerical integration from the fluorescence emission spectrum of PM-CaM and the absorption spectrum of nitrotyrosine CaM, as described previously (Yao et al., 1994). Color effects relating to the wavelength dependent properties of the photomultiplier were corrected using an algorithm provided by ISS Inc. (Urbana-Champaign, IL). In the presence of saturating calcium (pH 7.5), the quantum yield (ϕ_d) for PM-CaM is 0.175, and the overlap integral, J, for PM-nitrotyrosine-CaM is 2.80×10^{-15} M^{-1} cm^3. These constants were remeasured under the different experimental conditions used in this study and are reflected in the measured values of R_o (Table 4).

The above analysis assumes a unique donor−acceptor separation in the calculation of molecular distances, and ignores any conformational heterogeneity associated with the molecular dynamics of CaM. However, the intensity decay associated with the donor in the presence of an acceptor permits one to recover the conformational heterogeneity (or distribution of distances) associated with CaM [Haas et al., 1978; Beechem & Haas, 1989; Buckler et al., 1995; reviewed by Cheung (1991)]. To minimize the number of parameters, a uniform Gaussian distribution of donor to acceptor distances is often assumed

$$P(r) = \exp\left[-\frac{1}{2}\left(\frac{r - R_{av}}{\sigma}\right)^2\right] \tag{10}$$

where R_{av} is the average distance and σ is the standard deviation of the distribution. The width of the distribution is reported as the full-width at half-maximum (half-width, HW), which is given by HW = 2.354σ. The adequacy of the Gaussian model is assessed through a comparison of the goodness of the fit (i.e., χ_R^2, see below) relative to the fit using the more general multiexponential model which assumes no physical model.

Evaluation of Probable Errors in the Measurement of Molecular Distances using Fluorescence Resonance Energy Transfer. In the interpretation of the fluorescence resonance energy transfer data in terms of molecular distances it is typical to assume that the orientation between the donor and acceptor chromophores is motionally averaged during the excited state lifetime of the chromophore (i.e., $\kappa^2 = {}^2/_3$), and the influence of restrictions in the motional freedom of both donor and acceptor chromophores is typically the major concern associated with the interpretation of the experimental data. Direct measurements relating to the mobility of the chromophores through the measurements of either the steady-

state or time-resolved anisotropy (or polarization) provides a conservative estimate regarding the uncertainty in the apparent distance and suggests that, for chromophores in which the steady-state polarization is less than 0.2, the typical errors in the distance between chromophores is on the order of 5%−10% (Hass et al., 1978; Hahn & Hammes, 1978). This above estimate of the errors associated with FRET are consistent with previous measurements involving CaM, in which the use of two different FRET donors (covalently attached to Cys_{27}) with varying physical properties reveal similar average distances between and nitrotyrosine$_{139}$ that differ by less than 3 Å (Yao et al., 1994).

Decays of Fluorescence Anisotropy. As previously described (Lakowicz & Gryczynski, 1991; Johnson & Faunt, 1992), the time-resolved anisotropies were measured using the differential phase ($\Delta_\omega = \phi_\perp - \phi_{||}$) and modulated anisotropy ($r_\omega = [\Lambda_\omega - 1]/[\Lambda_\omega + 2]$), where $\Lambda = m_{||}/m_\perp$. The parameters describing the anisotropy decay were obtained from a least-squares fit to a multiexponential model, where

$$r(t) = r_0 \sum_i^n e^{-t/\phi_i} \tag{11}$$

r_0 is the limiting anisotropy in the absence of rotational diffusion, ϕ_i are the rotational correlation times, $r_0 g_i$ are the amplitudes of the total anisotropy loss associated with each rotational correlation time, and n is the total number of components associated with the exponential decay. The goodness of fit was determined through a comparison of the deviations between the measured and calculated values. Errors in Δ_ω and Λ_w were assumed to be 0.2 and 0.005, respectively.

Calculation of Expected Rotational Correlation Times. The expected rotational correlation times for proteins of variable shape have been discussed in detail [Garcia de la Torre & Bloomfield, 1981; reviewed by Steiner (1991)]. In the case of spherical proteins

$$D_r = \frac{kT}{6V\eta} \tag{12}$$

where D_r is the rotational diffusion coefficient, k is Boltzmann's constant, T is the absolute temperature in K, V is the hydrated volume of the protein of interest assuming two shells of bound water, and η is the solvent viscosity (0.89 cP at 25 °C). In the case of proteins that can be approximated as prolate ellipses, the rate of rotational diffusion about the two principal axis (i.e., $D_{||}$ and $D_\perp$) is related to the axial ratio (γ) of the protein of interest, such that

$$D_{||} = \frac{3\gamma(\gamma - \beta)}{2(\gamma^2 - 1)} D_r$$

where

$$\beta = (\gamma^2 - 1)^{-1/2} \ln(\gamma + (\gamma^2 - 1)^{1/2}) \tag{13}$$

and

$$D_\perp = \frac{3\gamma(2\gamma^2 - 1)\beta - \gamma}{2(\gamma^4 - 1)} D_r \tag{14}$$

The observed correlation times are predicted to be

$$\phi_a = \frac{1}{6D_\perp}$$

$$\phi_b = \frac{1}{5D_\perp + D_{||}}$$

$$\phi_c = \frac{1}{2D_\perp + 4D_{||}} \tag{15}$$

In the case of CaM complexed to CaMKII (Meador et al., 1993), the volume of hydrated CaM (using two shells of water; Cantor & Schimmel, 1980) is 33.75 nm^3, implying that $D_r = 2.3 \times 10^7$ s^{-1} at 25 °C in water. Assuming an axial ratio (γ) of 2.3 (which is consistent with the crystal structure of CaM bound to a peptide homologous to the autoinhibitory domain of CaMKIIα; Meador et al., 1993), this implies that $D_{||} = 1.45 \times 10^7$ s^{-1} and $D_\perp = 1.83 \times 10^7$ s^{-1}, and the associated correlation times are $\phi_a = 9.1$ ns, $\phi_b = 9.4$ ns, and $\phi_c = 10.6$ ns. However, one is generally unable to resolve the three rotational correlation times associated with the diffusion of a protein about the two principal axis due to both geometrical considerations involving the selective excitation of the transition dipole of the chromophore and due to the lack of experimental resolution (Small & Anderson, 1988).

RESULTS

Synthetic peptides that are homologous to sequences within the autoinhibitory domains of CaM-activatable proteins bind to CaM in a calcium-dependent manner with a similar stoichiometry and high affinity as observed for native proteins (Kemp et al., 1987; Blumenthal & Krebs, 1988; Payne et al., 1988) and are frequently used as a model system to obtain mechanistic information relating to CaM's ability to bind and to activate many different target proteins that possess little sequence homology [reviewed by Crivici and Ikura (1995); James et al., 1995]. In order to assess general features of the binding mechanism between CaM and target proteins that are regulated by CaM association, our strategy is to use frequency-resolved FRET to measure the spatial separation between the opposing globular domains of CaM bound to a range of target peptides that are homologous to the CaM binding sequences of CaM-regulated proteins. In addition, we have assessed the structure of CaM in association with melittin, an amphipathic peptide that binds CaM. These target peptides have little sequence similarity with respect to one another (Table 1), and therefore a comparison of the structure of CaM complexed to these various target peptides will provide valuable information relating to the mechanisms that allow CaM to bind and activate structurally diverse target proteins. These measurements take advantage of the single cysteine and tyrosine present in wheat germ CaM (Figure 1), which can be modified to provide fluorescence signals that serve to monitor structural changes associated with peptide binding to CaM, as discussed previously (Yao et al., 1994). Wheat germ CaM has 90% sequence identity with bovine CaM (Klee et al., 1980; Toda et al., 1985) and previously has been shown to fully activate a range of proteins from human and animal sources (Strasburg et al., 1988; Yao et al., 1994).

CaM Binding to Peptides That Are Homologous to the Autoinhibitory Domains of CaM-Regulated Proteins. The

Table 1: Primary Sequences of Target Peptides and Associated Binding Energies for CaM

target	sequences[a]	$\Delta G'$ (kcal mol^{-1})[b]
RS20	A R R K W Q K T G H A V R A I G R L S S	-9.2 ± 0.1
CAMKII20	K K F N A R R K L K G A I L T T M L A	-11.4 ± 0.7
C25W	Q I L W F R G L N R I Q T Q I R V V N A F R S S C	-9.2 ± 0.1
F52	K K K K K F S F K K P F K L S G L S F K R N R K	-9.2 ± 0.2
PHK5	L R R L I D A Y A F R I Y G H W V K K G Q Q Q N R G	-9.2 ± 0.1
Melittin	G I G A V L K V L T T G L P A L I S W I K R K R Q Q	-9.5 ± 0.1

[a] Peptide alignment emphasizes conserved hydrophobic amino acids (underlined) of the peptide, as suggested previously (Meador et al., 1993; Crivic & Ikura, 1995). [b] Binding energies were calculated as described in Experimental Procedures, where $\Delta G = -RT \ln(K_a)$. K_a is the association constant, T is the absolute temperature in K, and R is the gas constant.

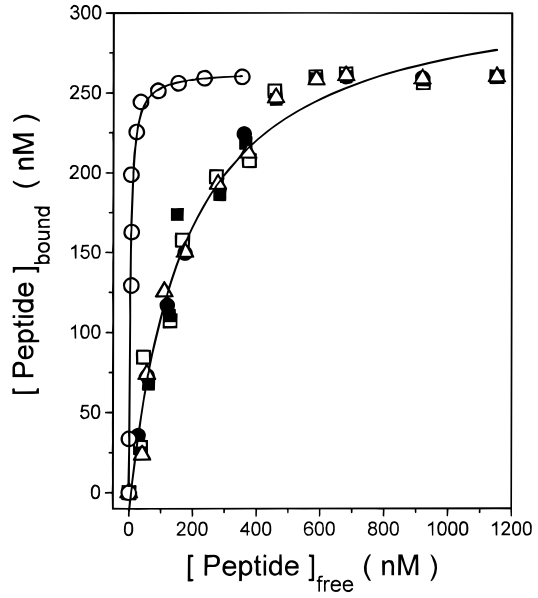

FIGURE 2: Binding affinities of target peptides to CaM. The binding affinity between CaM and peptides that are homologous to the CaM binding sequences of a range of CaM-regulated proteins. These peptides include CaMKII (○), PHK5 (●), F52 (□), RS20 (■), and C25W (△) was measured using the associated decrease in the steady-state fluorescence of pyrene maleimide labeled CaM upon peptide binding. The respective decreases in steady-state fluorescence were 25% ± 2% (CaMKII), 29% ± 1% (PHK5), 30% ± 2% (F52), 29% ± 2% (RS20), and 28% ± 1% (C25W). In the case of melittin there was a 32% ± 1% decrease in steady-state fluorescence upon peptide binding (data not shown). Lines represent nonlinear least-squares fits to the data using eq 3 in Experimental Procedures. Titrations were carried out in 0.1 M HEPES (pH 7.5), 0.1 M KCl, 1 mM $MgCl_2$, and 0.1 mM $CaCl_2$ at 25 °C. Total CaM concentration was 0.26 μM.

affinity of CaM for six different target peptides was measured using the decrease in the fluorescence of pyrene maleimide (PM) labeled CaM upon peptide binding (Figure 2). We observe a 25%−32% decrease in the steady-state fluorescence of PM-labeled CaM depending on the target peptide, indicating that there are analogous structural changes associated with the environment around PM located at Cys_{27} on CaM irrespective of the peptide target. The majority of target peptides have very similar binding affinities for CaM (i.e., $\Delta G' \approx -9$ kcal mol^{-1}; Table 1); however, CaMKII20 has a substantially higher affinity (i.e., $\Delta G' \approx -11$ kcal mol^{-1}; Table 1).

Measurements of the Fluorescence Lifetime of PM-CaM. In order to assess possible differences in the conformation of CaM bound to target peptides we have measured the lifetime of PM-CaM complexed to all six target peptides using frequency-domain fluorescence spectroscopy. PM is located at Cys_{27} in calcium binding loop I in CaM. The lifetime and solvent accessibility of PM-CaM have previously been shown to be very sensitive to the structural changes associated with calcium activation of CaM (Yao et al., 1994). The phase lag and demodulation of intensity-modulated light was measured at 20 frequencies between 0.4 and 90 MHz for both calcium-activated CaM and subsequent to peptide binding (Figure 3). In all cases the peptide concentrations were chosen so as to fully saturate the CaM binding sites but were sufficiently low to avoid nonspecific interactions between CaM and target peptides (Table 2). Upon peptide binding we observe that the frequency-response of PM-CaM shifts toward higher frequencies (compare open symbols in Figure 3A,B), indicating that the average lifetime of PM decreases upon peptide binding (Table 2).

The intensity decay of PM-CaM can be adequately described as a sum of three exponentials, as indicated by the random distribution of the weighted residues about the origin (Figure 3). In all cases there was a greater than 10-fold improvement in the goodness of fit (i.e., χ_R^2) for a model involving three exponentials relative to the two-exponential model (Table 2), indicating that this model is statistically justifiable. Inclusion of additional fitting parameters results in no further improvement of χ_R^2.

The fluorescence lifetime of pyrene maleimide is very sensitive to the surrounding protein environment, and the observed decrease in the lifetime of PM-CaM upon peptide binding is related to alterations in the tertiary structure of CaM (Royer, 1993). We observe that there is a large decrease in the average lifetime of PM-CaM upon peptide binding, which in the case CaMKII20 changes from 13.5 ± 0.6 ns to 3.8 ± 0.2 ns. The lifetime of PM-CaM upon CaMKII20 peptide binding is similar to that of both free probe and for PM-CaM after denaturation with GnHCl ($\tau \approx$ 3.8 ns; Table 3), suggesting that upon peptide binding the local environment around Cys_{27} becomes more solvent accessible. This suggestion is consistent with the exposed position of the analogous amino acid (i.e., Thr_{26}) observed in the crystal structure of vertebrate CaM bound to this target peptide (Meador et al., 1993). However, while the average lifetime of PM-CaM bound to the five other target peptides used in this study is similar to that observed for CaMKII20, there is significant variation in the average lifetime ranging from 5.6 ± 0.2 ns for F52 to 2.8 ± 0.1 ns for melittin (Table 2). The variable lifetimes observed for these peptide−CaM

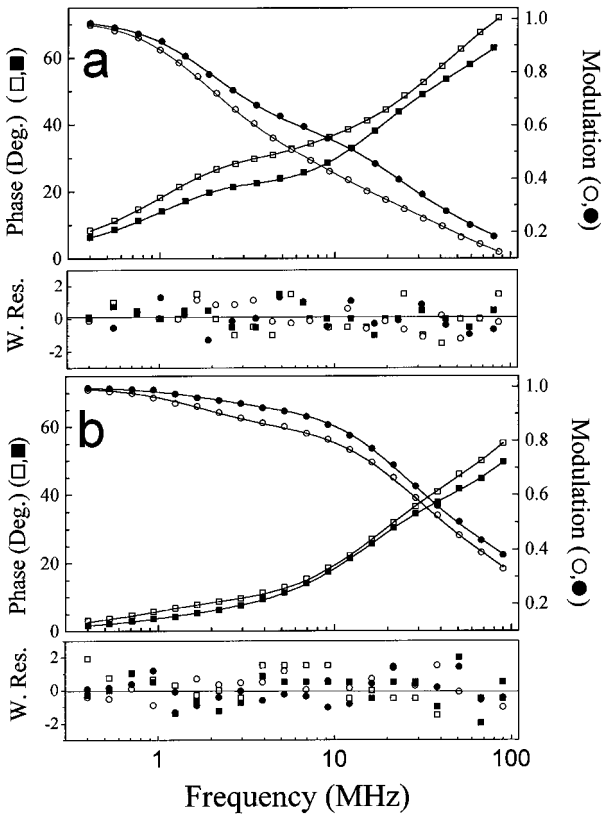

FIGURE 3: Lifetime data relating to fluorescence resonance energy transfer between PM located at Cys_{27} and nitrotyrosine$_{139}$ in CaM. The frequency response of the phase shift (□, ■) and demodulation (○, ●) of frequency-modulated light for PM-CaM (i.e., donor only; □, ○) and for PM-CaM in the presence of nitrotyrosine (i.e., donor−acceptor; ■, ●) in the presence of saturating calcium (panel a) and subsequent to the addition of 1.7 μM CaMKII (panel b). Solid lines represent the best fit to the data, as described in Experimental Procedures. Below each data set are the weighted residuals, which correspond to the difference between the experimental data and the experimental fit normalized by the experimental error associated with the phase (i.e., $\delta_{phase} = 0.2°$) and modulation (i.e., $\delta_{mod} = 0.005$), which were assumed to be frequency-independent. In all cases measurements were made in 0.1 M HEPES (pH 7.5), 0.1 M KCl, 1 mM $MgCl_2$, and 0.1 mM $CaCl_2$ at 25 °C. Total CaM concentration is 1.1 μM.

complexes relative to that observed for CaMKII20 indicate differences in the conformation of the environment surrounding PM that is dependent on the target peptide, and may be related to the interaction between the amino-terminal domain of CaM and the length of the carboxyl-terminus of these peptides, which have the potential to decrease the solvent exposure of PM at Cys_{27} (see below). The average lifetime of CaM complexed with melittin is 2.8 ± 0.1 ns, which is substantially less than that observed for the free probe in solution. The very short lifetime of PM-CaM complexed with melittin may be related to the large charge density near the carboxyl-terminus of melittin, which may both alter the conformation of the peptide relative to CaM and modify the excited-state characteristics of pyrene (Lakowicz, 1983).

Peptide Binding Induces Changes in Probe Accessibility. The underlying reasons for the differences in the average lifetime of PM-CaM associated with binding the six target peptides was further investigated using the water soluble quencher TEMPAMINE to assess the exposure of bound PM relative to that of free PM in solvent. TEMPAMINE has the advantage of greater quenching efficiency relative to other commonly used quenchers (i.e., KI and acrylamide), thereby

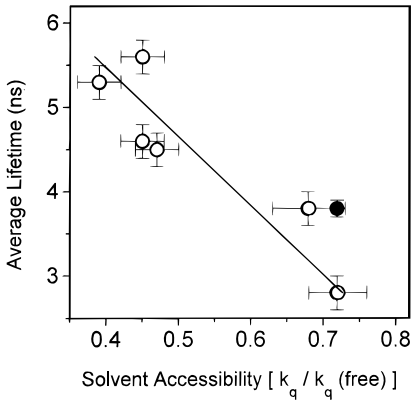

FIGURE 4: Relationship between solvent accessibility and average lifetime of PM-CaM complexed with target peptides. The average lifetime and the associated solvent accessibility of PM-CaM complexed with each of the six target peptides (○) or PM-CaM denatured in 6.0 M GnHCl (●) are directly compared. The line represents a fit to the data assuming a linear function, where the slope is −6.7 ± 1.5, the intercept is 8.0 ± 0.8, and the correlation coefficient is −0.91. The experimental conditions and the corrections necessary to calculate the solvent accessibility of PM-CaM in 6.0 M GnHCl are described in Table 3.

allowing us to access the solvent accessibility of PM without significantly altering the ionic strength. A comparison of the solvent accessibility of PM-CaM bound to the respective target peptides provides a very sensitive measurement of differences in the local tertiary structure of CaM near PM (Schöneich et al., 1995) and permits a quantitative assessment of the variable average lifetimes associated with PM-CaM bound to target peptides (see above), since static quenching interactions that may involve local changes in the proximity of specific functional groups in the vicinity of PM can be distinguished from large scale changes in the overall conformation of the amino-terminal domain of CaM.

Irrespective of the target peptide, we observe a 3- to 5-fold increase in the solvent accessibility of PM-CaM upon binding target peptides relative to calcium-saturated CaM (Table 3). The enhanced solvent accessibility of PM located at Cys_{27} in CaM is consistent with the decreased lifetime of PM upon binding target peptides (see above), and is in agreement with the greater exposure of the equivalent amino acid (i.e., Thr_{26}) in vertebrate CaM upon binding the target peptides RS20 or CaMKII (Meador et al., 1992, 1993; Ikura et al., 1992). One observes a good correlation between the lifetimes of PM-CaM bound to each of the six target peptides and their associated solvent accessibilities (Figure 4). Thus the observed variation in the lifetime of PM-CaM bound to each of the various target peptides is a reflection of differences in solvent accessibility, and is not the result of alterations in specific quenching interactions with neighboring amino acids. Therefore, the observed variation in both the average lifetime and solvent accessibility of PM-CaM upon binding different target peptides arises as a result of differences in the conformation around Cys_{27} upon binding the six different target peptides. This result is consistent with previous evidence relating to the plasticity of the globular domains in CaM with respect to their ability to bind the variable target sequences associated with peptides that are homologous to the CaM binding sequences of both myosin light-chain kinase (RS20) and calmodulin-dependent protein kinaseIIα (CaMKII; Meador et al., 1992, 1993).

Spatial Separation between Globular Domains. In order to quantitatively assess the conformation of CaM bound to

Table 2: Lifetime Data Associated with Peptide Binding to CaM[a]

sample	conditions		α_1	τ_1 (ns)	α_2	τ_2 (ns)	α_3	τ_3 (ns)	$\bar{\tau}$ [b] (ns)	χ_R^2 [c]
A. CaM	$+Ca^{2+}$	D	0.79 ± 0.02	3.75 ± 0.10	0.137 ± 0.005	18.6 ± 0.4	0.076 ± 0.003	106 ± 5	13.6 ± 0.6	0.7 (7.9)
		DA	0.76 ± 0.02	2.26 ± 0.08	0.174 ± 0.006	11.3 ± 0.3	0.066 ± 0.002	74 ± 4	8.6 ± 0.3	1.3 (22.1)
	+6 M GnHCl	D	0.47 ± 0.03	1.36 ± 0.07	0.507 ± 0.014	4.7 ± 0.1	0.019 ± 0.001	43 ± 2	3.8 ± 0.1	0.51 (11.6)
		DA	0.54 ± 0.02	1.27 ± 0.07	0.438 ± 0.011	4.7 ± 0.1	0.018 ± 0.001	37 ± 2	3.4 ± 0.1	0.60 (9.9)
B. CaM + peptide	RS20	D	0.68 ± 0.01	1.70 ± 0.08	0.304 ± 0.011	6.8 ± 0.3	0.013 ± 0.001	104 ± 4	4.6 ± 0.2	1.3 (14.3)
		DA	0.70 ± 0.02	1.03 ± 0.05	0.291 ± 0.010	6.5 ± 0.2	0.010 ± 0.001	94 ± 3	3.5 ± 0.1	0.82 (11.2)
	CaMKII20	D	0.71 ± 0.02	1.64 ± 0.07	0.284 ± 0.010	7.4 ± 0.2	0.006 ± 0.001	98 ± 4	3.8 ± 0.2	1.0 (13.4)
		DA	0.78 ± 0.02	1.32 ± 0.05	0.223 ± 0.008	7.7 ± 0.2	0.003 ± 0.001	87 ± 3	3.0 ± 0.1	0.75 (10.2)
	+C25W	D	0.78 ± 0.01	2.14 ± 0.08	0.200 ± 0.008	9.8 ± 0.4	0.016 ± 0.001	104 ± 4	5.3 ± 0.2	1.5 (7.9)
		DA	0.78 ± 0.02	1.54 ± 0.06	0.200 ± 0.007	7.3 ± 0.3	0.016 ± 0.001	76 ± 3	3.9 ± 0.2	1.3 (11.9)
	+F52	D	0.78 ± 0.02	2.23 ± 0.02	0.203 ± 0.008	10.2 ± 0.4	0.017 ± 0.001	107 ± 4	5.6 ± 0.2	1.6 (15.6)
		DA	0.78 ± 0.02	1.25 ± 0.05	0.205 ± 0.007	6.2 ± 0.2	0.015 ± 0.001	66 ± 3	3.2 ± 0.1	2.3 (19.3)
	+PHK5	D	0.73 ± 0.02	1.27 ± 0.05	0.252 ± 0.008	8.9 ± 0.3	0.015 ± 0.001	89 ± 3	4.5 ± 0.2	0.43 (1.3)
		DA	0.72 ± 0.01	1.14 ± 0.04	0.270 ± 0.010	7.6 ± 0.3	0.012 ± 0.001	86 ± 4	3.9 ± 0.1	0.81 (3.6)
	+melittin	D	0.80 ± 0.02	1.21 ± 0.04	0.193 ± 0.006	7.8 ± 0.2	0.006 ± 0.001	59 ± 2	2.8 ± 0.1	1.1 (12.2)
		DA	0.74 ± 0.02	0.59 ± 0.02	0.246 ± 0.007	4.7 ± 0.1	0.011 ± 0.001	32 ± 1	2.0 ± 0.1	0.86 (9.3)

[a] Average amplitudes (α_i) and lifetimes (τ_i) obtained from three-exponential fits to frequency-domain data collected for donor only (D or PM-CaM)- and donor−acceptor (DA or PM-nitrotyrosine-CaM)-labeled calmodulin, where uncertainties represent the maximal variance associated with a rigorous analysis of the correlated errors between the five fitting parameters relative toi the parameter of interest, as previously described (Beechem et al., 1991; Yao et al., 1994). [b] The amplitude weighted average lifetime ($\bar{\tau}$) is calculated as $\bar{\tau} = \sum \alpha_i \tau_i$ and is proportional to the quantum yield of PM-CaM (Leudtke et al., 1981). The associated errors were propagated as described in Begington (1969), where

$$\sigma_{\bar{\tau}}^2 = \sum_i \sigma_{\alpha_i \tau_i}^2 \text{ and } \sigma_{\alpha_i \tau_i}^2 = ((\sigma_{\alpha_i}^2/\alpha_i^2) + (\sigma_{\tau_i}^2/\tau_i^2))(\alpha_i \tau_i)^2$$

[c] The χ_R^2 for a two-exponential fit to the data is shown in brackets for comparison purposes. The medium buffer contained 0.1 M HEPES (pH 7.5), 0.1 M KCl, 1 mM $MgCl_2$, and 0.1 mM $CaCl_2$. The temperature was 25 °C. The concentration of CaM was 1.2 μM, and when applicable the concentration of CaMKII20 was 1.7 μM. The concentration of other peptides was 3.6 μM in all cases.

Table 3: Solvent Accessibility of PM-CaM[a]

sample	conditions	K_{sv} (M^{-1})[b]	$\bar{\tau}$ (*ns*)[c]	k_q (M^{-1} s^{-1})[c]	k_q [d] / k_q(free probe)
A. free probe[e]		385 ± 22	3.9 ± 0.2	$(99 \pm 5) \times 10^9$	1.0 ± 0.05
B. CaM[e]	+ Ca^{2+}	182 ± 11	13.6 ± 0.5	$(13 \pm 1) \times 10^9$	0.13 ± 0.01
	+ 6 M GnHCl	163 ± 10	3.8 ± 0.1	$(43 \pm 2) \times 10^9$	0.43 ± 0.02[f]
C. CaM + peptide	+ RS20	210 ± 12	4.6 ± 0.2	$(46 \pm 3) \times 10^9$	0.46 ± 0.03
	+ CaMKII20	267 ± 16	3.9 ± 0.2	$(68 \pm 5) \times 10^9$	0.68 ± 0.05
	+ C25W	207 ± 13	5.3 ± 0.3	$(39 \pm 3) \times 10^9$	0.39 ± 0.03
	+ F52	228 ± 14	5.6 ± 0.2	$(45 \pm 3) \times 10^9$	0.45 ± 0.03
	+ PHK5	205 ± 13	4.5 ± 0.2	$(46 \pm 3) \times 10^9$	0.46 ± 0.03
	+ melittin	201 ± 11	2.8 ± 0.1	$(72 \pm 4) \times 10^9$	0.72 ± 0.04

[a] Protein conformational changes are revealed by changes in solvent accessibility of the water soluble quencher TEMPAMINE to pyrene maleimide associated with Cys_{27} in CaM. [b] K_w is obtained from the Stern−Volmer relationship $F_0/F = 1 + K_{sv}$[TEMPAMINE], where F_0 is the initial fluorescence intensities in the absence of added quenchers. [c] $k_q \equiv K_{sv}/\bar{\tau}$, where $\bar{\tau} \equiv \sum \alpha_i \tau_i$ (see Table 2). [d] The quenching efficiency of the chromophore bound to CaM was normalized to that of the free probe in buffer. [e] Values taken from Yao et al. (1994), where free probe is PM-CaM in medium buffer (see below). [f] k_q/k_q(free probe) corrected for the viscosity of 6 M GnHCl ($\eta = 1.624$ cP) relative to pure water ($\eta = 0.89$ cP) is 0.70. Experimental conditions: The concentration of CaM and target peptides were 1.2 and 3.6 μM, respectively, except for the target peptide CaMKII20 whose concentration was 1.7 μM. The medium buffer contained 0.1 M HEPES (pH 7.5), 0.1 M KCl, 1 mM $MgCl_2$, and 0.1 mM $CaCl_2$. The temperature was 25 °C.

target peptides we have used FRET between PM located at Cys_{27} and nitrotyrosine$_{139}$ to measure the spatial separation between the opposing globular domains in CaM upon association with target peptides (Figure 1). A comparison of either the steady-state fluorescence intensity (data not shown) or average lifetime of the FRET donor PM in the presence and absence of the FRET acceptor nitrotyrosine (Table 2) and a knowledge of the Förster critical distance (R_0) under the conditions of interest permit a measurement of the apparent donor−acceptor separation (r_{app}; eq 8 in Experimental Procedures), which neglects any conformational heterogeneity in CaM by assuming a single donor−acceptor distance. In all cases the observed changes in the steady-state emission spectrum and average fluorescence lifetime ($\bar{\tau}$) of PM-CaM upon nitration of Tyr_{139} are virtually identical, indicating that the sample is homogeneous and that there is essentially no nonspecific binding between CaM polypeptide chains in solution. However, our measurements emphasize the use of fluorescence lifetime measurements due to the enhanced information content contained in the time-dependent decays of fluorescence intensity (see below).

Upon nitration of Tyr_{139} the frequency response of PM-CaM is shifted to higher frequencies for both calcium-saturated CaM (Figure 3A) and for CaM bound to target peptides (e.g., Figure 3B), indicating a shorter average lifetime ($\bar{\tau}$) of PM-CaM in the presence of the FRET acceptor nitrotyrosine. There is a relatively small (i.e., 5.5 ± 0.9 Å) variation in the apparent spatial separation between these donor−acceptor pairs bound to all six peptides, which varies between 17.9 ± 0.4 Å for melittin to 23.4 ± 0.8 Å for PHK5. The observed variation in the spatial separation between the opposing globular domains in CaM upon binding target

Table 4: Donor−Acceptor Separation between Chromophores on Opposing Globular Domains of Calmodulin[a]

sample	conditions	E (%)[b]	R_0 (Å)[c]	r_{app} (Å)[d]	R_{av} (Å)[e]	HW (Å)[e]	χ_R^2
A. CaM	$+Ca^{2+}$	36.8 ± 1.7	20.6 ± 0.1	22.5 ± 0.5	22.4 (21.8−23.4)	11.8 (10.8−14.0)	3.5
	+6 M GnHCl[f]	11.4 ± 0.2	17.6 ± 0.1	24.5 ± 0.3	26.0 (25.6−26.3)	22.5 (17.9−26.8)	2.2
B. CaM + peptide	+ RS20	22.4 ± 1.1	17.2 ± 0.1	21.2 ± 0.6	19.9 (19.3−20.7)	7.7 (6.5−8.9)	2.2
	+ CaMKII20	21.8 ± 1.7	16.7 ± 0.1	20.7 ± 0.7	19.5 (19.1−20.0)	8.1 (6.4−9.7)	2.9
	+C25W	26.9 ± 1.8	17.6 ± 0.1	20.8 ± 0.6	20.9 (20.6−21.2)	8.5 (7.4−9.8)	1.6
	+F52	42.9 ± 2.2	17.8 ± 0.1	18.7 ± 0.6	18.5 (18.3−18.7)	6.2 (5.0−7.7)	1.7
	+ PHK5	13.5 ± 0.6	17.2 ± 0.1	23.4 ± 0.8	21.9 (21.0−22.5)	8.9 (7.5−10.4)	2.0
	+ melittin	31.0 ± 1.1	15.7 ± 0.1	17.9 ± 0.4	19.5 (19.3−20.1)	7.2 (5.6−8.6)	2.5

[a] Distance measurements obtained from fluorescence resonance energy transfer (FRET) measurements between donor chromophores covalently associated with Cys_{27} and nitrotyrosine 139 in wheat germ CaM. [b] Observed energy-transfer efficiency is obtained from changes in the average fluorescence lifetime ($\bar{\tau}$) of PM-CaM upon nitration of Tyr_{139}, where $E = (1 - \bar{\tau}_{da}/\bar{\tau}_d)$ and is multiplied by 100. Errors are the standard deviation of the mean. [c] The Förster critical distance represents the distance between a given donor−acceptor pair under a given set of experimental conditions where the energy-transfer efficiency is 50%. Indicated errors represent the standard deviation of the mean. [d] The apparent donor-acceptor separation was calculated using eq 8 in Methods, and assumes that the protein exists in a unique conformation. The indicated errors are propaged (Bevington, 1969). [e] The average donor−acceptor separation (R_{av}) and associated half-width at half-height (HW) assume that the distribution of distances between donor and acceptor chromophores can be approximated using a Gaussian distribution of distances and are calculated using eq 10 in Experimental Procedures. Indicated errors (in brackets) were obtained from a rigorous analysis of the error surfaces associated with each experimental parameter (Beechem et al., 1991; Yao et al., 1994). Experimental conditions: the CaM concentration was 1.2 μM. When applicable, the concentration of CaMKII20 was 1.7 μM. All other peptides were added at a concentration of 3.6 μM. The medium buffer contained 0.1 M HEPES (pH 7.5), 0.1 M KCl, 1 mM $MgCl_2$, and 0.1 mM $CaCl_2$. The temperature was 25 °C. [f] From Yao et al. (1994).

peptides is consistent with the proposed role of the flexible central helix in allowing CaM to bind to a range of target peptides with variable binding sequences (Ikura et al., 1992).

The average donor−acceptor separation decreases from 23 Å in calcium-saturated CaM to about 21 Å in the case of CaM bound to either CaMKII or RS20 (Table 4). The observed decrease in donor−acceptor separation associated with peptide binding is consistent with the 3 Å decrease in the distance between the analogous amino acid residues in vertebrate CaM (i.e., Thr_{26} and Tyr_{138}) observed in the crystal structures of calcium-saturated CaM relative to CaM bound to these two target peptides [Babu et al., 1985; 1988; Chattopadhyaya et al., 1992; Meador et al., 1992; 1993; reviewed by Crivici and Ikura (1995)].

Conformational Heterogeneity of CaM Bound to Target Peptides. The time-dependent decay of FRET contains information relating to the conformational heterogeneity of macromolecules [Hass et al., 1978; Beechem & Haas, 1989; reviewed by Cheung (1991)]. We have therefore used the frequency domain intensity decays of PM-CaM in the presence and absence of nitrotyrosine to recover the time-dependent terms relating to the distribution of distances between the two opposing globular domains of CaM bound to all six target peptides (Table 4). We observe that the average donor−acceptor distance (R_{av}) recovered from the distance distribution model (eq 10 in Experimental Procedures) is analogous to the results obtained using average lifetimes to calculate apparent distances between PM at Cys_{27} and nitrotyrosine$_{139}$ (eq 8 in Experimental Procedures; Table 4). The average donor−acceptor separation between these chromophores for all six peptides is close to 20 Å and ranges from 18.6 Å (F52) to 21.9 Å (PHK5). While there is a 3 ± 1 Å variation in the average donor−acceptor distances (R_{av}) upon binding target peptides (compare PHK5 and melittin; Table 4), in all cases we observe that the half-width of the distance distribution is very similar for all target peptides (i.e., 7−8 Å) and is much narrower than the half-width of the distance distribution for calcium-saturated CaM (i.e., ∼12 Å; Figure 5), indicating less conformational heterogeneity between the opposing globular domains of CaM. The similar degree of conformational heterogeneity between the opposing globular domains of CaM bound to each of the six target

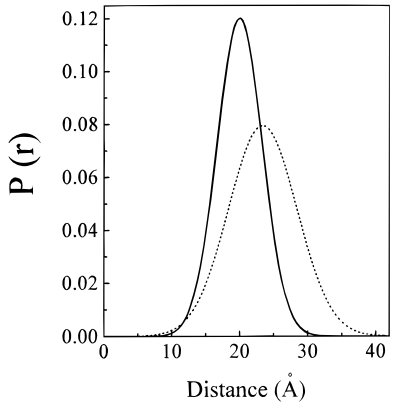

FIGURE 5: Distance distribution between donor and acceptor chromophores located in opposing globular domains in CaM. Depiction of distribution of distances calculated between donor (i.e., pyrene maleimide located at Cys27 in calcium binding site I) and acceptor (i.e., nitrotyrosine$_{139}$ located in calcium binding site IV) assuming a uniform Gaussian distance distribution for calcium-saturated CaM (dotted line) and subsequent to the association of CaM with the target peptides (solid line). In the latter case the indicated distribution represent the average separation and half-width observed for all six peptides (Table 4). The distance distribution associated with calcium-saturated CaM have been previously discussed (Yao et al., 1994) and are shown for comparison purposes. Sample conditions: 1.13 μM PM-CaM in 0.1 M HEPES (pH 7.5), 0.1 M KCl, 1 mM $MgCl_2$, and 0.1 mM $CaCl_2$ (dotted line). The sample temperature was 25 °C.

peptides is consistent with previous results that suggest that all six of these target peptides adopt α-helical structures upon association with target peptides (Blackshear et al., 1982; Maulet & Cox, 1983; Seeholzer et al., 1986; Dasgupta et al., 1989; Kataoka et al., 1991; Meador et al., 1992, 1993), since the secondary structure of the bound peptides should alter both the time-dependent spatial separation between the CaM binding sites and the associated dynamics of the complex between CaM and target peptides (see below).

From the above discussion, it is evident that the apparent and average distances between PM at Cys_{27} and nitrotyrosine$_{139}$ are substantially less than the minimum distances between these analogous amino acid side chains in the crystal structures of both calcium-saturated CaM and CaM associated with target peptides. However, from an assessment of

the conformational heterogeneity obtained from an analysis of the time-dependent FRET observed in this study in which the separation between Cys_{27} and $nitrotyrosine_{139}$ is fit assuming a Gaussian distance distribution, we find that the maximum separation between these chromophores is in good agreement with the separation between the C_α carbons in the analogous amino acid side chains observed in the crystal structure (i.e., 38 Å for calcium-saturated CaM; 33 Å for CaM bound to the peptides RS20 and CaMKII). Therefore, the decrease in the average separation between these chromophores observed using FRET is consistent with the presence of conformational heterogeneity in solution. In this respect it should be remembered that the crystal structures were obtained at low pH in the presence of helicogenic solvents that may predispose CaM to adopt a more fully extended average structure. Furthermore, the high-field NMR and crystal structures of CaM are only sensitive to conformations of CaM that are both heavily populated and very long-lived (Bajzer & Prendergast, 1993).

Rotational Dynamics of CaM upon Binding Target Peptides. We have used frequency-domain measurements of fluorescence anisotropy of PM-CaM to assess dynamic conformational changes of CaM upon binding target peptides. These measurements allow us to assess both (i) segmental motion associated with PM at Cys_{27} and (ii) the overall rotational motion of CaM upon association with target peptides. Segmental motion provides information relating to the local environment around the chromophore and provides complementary information to the lifetime and quenching measurements, while global rotational motion is sensitive to the overall dimensions of the CaM-peptide complex.

In our measurements we collected differential phase and modulated anisotropy data over 18 frequencies between 0.6 and 90 MHz (Figure 6). One observes that there are substantial differences in the frequency response of both the differential phase (Figure 6A) and modulated anisotropy (Figure 6B) for calcium-saturated CaM relative to CaM bound to target peptides. The increased modulated anisotropy observed for CaM associated with CaMKII20 at low frequencies (which corresponds to the remaining polarization at long times relative to the excited state lifetime of PM) is consistent with the substantial increase in the steady-state polarization of PM-CaM upon association with CaMKII20, which increases from 0.078 ± 0.002 to 0.156 ± 0.002 (Table 5).

In all cases, a sum of two exponentials adequately describes the anisotropy data associated with both calcium-saturated CaM and for CaM bound to target peptides, as judged by both the more than 20-fold reduction in the goodness of the fit (χ_R^2; Table 5) and the evenly distributed weighted residuals (Figure 6). Inclusions of additional fitting parameters results in no significant improvement in the calculated fit to the data. Therefore, we are able to resolve two correlation times (i.e., ϕ_1 and ϕ_2) associated with the rotational dynamics of PM-CaM. For both calcium-activated CaM and CaM bound to target peptides we observe analogous correlation times associated with segmental (ϕ_1) and global (ϕ_2) rotational motion (Table 5). The observed differences in differential phase and modulated anisotropy (Figure 6) are largely a reflection of the 3.5-fold reduction in the excited-state lifetime of PM associated with peptide binding, since the frequency response of the differential phase and the modulated anisotropy are dependent on the lifetime of chromophore of interest (Weber, 1981).

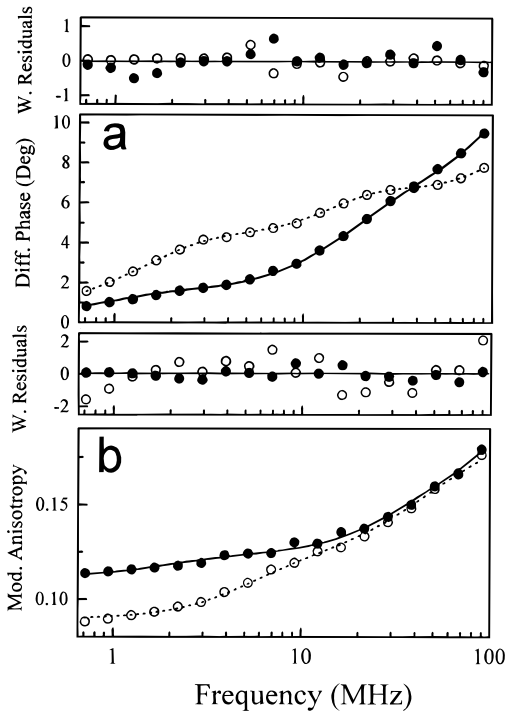

FIGURE 6: Rotational dynamics of pyrene maleimide labeled CaM. Frequency-domain anisotropy data and the respective least-squared fits to the data are shown for calcium-saturated CaM (○; dotted line) and subsequent to the association with CaMKII20 peptide (●; solid line) for both the differential phase (a) and modulated anisotropy (b). The weighted residuals (W. Residuals) are shown above each plot and represent the difference between the experimental and calculated values for the differential phase (a) and modulated anisotropy (b), normalized by the assumed errors for these respective measurements. The assumed errors for the phase and modulation are 0.2° and 0.005, respectively. The CaM concentration was 1.1 μM (i.e., 19 μg/mL) in 0.1 M HEPES (pH 7.5), 0.1 M KCl, 1 mM $MgCl_2$, and 0.1 mM $CaCl_2$. When appropriate 1.7 μM CaMKII was present in the solution. Temperature was 25 °C.

Segmental Rotational Dynamics. The amplitude (g_1r_0) and rate ($1/\phi_1$) of rotational motion associated with the segmental motion of PM-CaM bound to the target peptides RS20, CaMKII20, C25W, and F52 are virtually unchanged relative to calcium-activated CaM ($g_1r_0 \approx 0.17 \pm 0.02$; $\phi_1 \approx 0.8 \pm 0.1$ ns; see Table 5), consistent with earlier crystallographic evidence that the tertiary structure of the opposing globular domains in calcium-activated CaM is virtually unchanged upon binding the target peptides RS20 and CaMKII20 (Meador et al., 1992, 1993). However, upon association of PM-CaM with either PHK5 ($\phi_1 = 0.5 \pm 0.1$ ns) or melittin ($\phi_1 = 1.4 \pm 0.1$ ns) we observe significant differences in the rotational correlation times associated with segmental motion relative to the other target peptides. The altered segmental motion of PM-CaM bound to these target peptides indicates that the tertiary conformation of the amino-terminal domain of PM-CaM is different relative to the other four target peptides. This is consistent with the altered spatial separation between the two opposing globular domains of PM-CaM bound to these latter two target peptides ($r_{app} = 23.4 \pm 0.8$ for PHK5 and $r_{app} = 17.9 \pm 0.4$ for melittin), relative to the average donor−acceptor separation for CaM bound to the other four target peptides ($r_{app} = 20.2 \pm 2.0$; Table 4).

Table 5: Rotational Dynamics of Calmodulin Complexed with Target Peptides[a]

sample	conditions	P[b]	g_1r_0[c]	ϕ_1 (ns)[d]	g_2r_0[c]	ϕ_2 (ns)[d]	χ_R^2 [e]
A. CaM	+ Ca^{2+} [f]	0.078 ± 0.002	0.16 ± 0.01	0.8 ± 0.1	0.11 ± 0.01	10.9 ± 0.7	0.50 (20.4)
B. CaM + peptide	+ RS20	0.132 ± 0.002	0.17 ± 0.01	0.8 ± 0.1	0.11 ± 0.01	10.2 ± 0.7	0.63 (14.7)
	+ CaMKII20	0.156 ± 0.002	0.19 ± 0.01	0.7 ± 0.1	0.11 ± 0.01	10.6 ± 0.7	0.37 (8.6)
	+ C25W	0.138 ± 0.002	0.17 ± 0.01	0.9 ± 0.1	0.10 ± 0.01	10.3 ± 0.5	0.78 (10.4)
	+ F52	0.159 ± 0.003	0.17 ± 0.01	0.9 ± 0.1	0.10 ± 0.01	10.6 ± 0.6	0.65 (13.8)
	+ PHK5	0.127 ± 0.002	0.17 ± 0.01	0.5 ± 0.1	0.10 ± 0.01	11.2 ± 0.9	0.60 (11.5)
	+ melittin	0.144 ± 0.001	0.17 ± 0.02	1.4 ± 0.1	0.11 ± 0.01	10.4 ± 1.1	0.84 (15.6)

[a] Steady-state and time-resolved measurements of the rotational dynamics of pyrene maleimide were used to assess ligand-dependent changes in either the segmental (ϕ_1) or overall (ϕ_2) rotational dynamics of CaM. The reported correlation times and their associated amplitudes are obtained from a multiexponential fit to the experimental data using frequency-independent errors as described in Experimental Procedures. The indicated errors were obtained from a rigorous consideration of the errors and accounts for all correlations between the measured parameters (Beechem et al., 1991; Yao et al., 1994). This involved the systematic variation of the parameter of interest, allowing all other parameters to vary so as to minimize the χ_R^2 as described in Experimental Procedures. The reported uncertainty is obtained using the F statistic and represents the maximal variance associated with one standard deviation relative to the reported values. [b] P is the steady-state polarization (P), where $P \equiv (I_{||} - gI_{\perp})/(I_{||} + gI_{\perp})$. $I_{||}$ and $I_{\perp}$ refer to the steady-state fluorescence intensity obtained using vertically polarized light as an excitation source when the emission polarizer is in the vertical and horizontal directions, respectively. The$g$ factor corrects for imperfections in the polarizers, where upon exictation with horizontally polarized light $g \equiv I_{||}/I_{\perp}$. [c] g_ir_0 is the amplitude of the total anisotropy associated with each rotational correlation time (ϕ_i). [d] ϕ_1 and ϕ_2 are the rotational correlation times associated with segmental and overall protein rotational motion. [e] χ_R^2 describes the deviations between the model and experimental data (see Experimental Procedures). The numbr in parentheses represents the χ_R^2 obtained from a one-component fit to the data. [f] Data taken from Yao et al. (1994). Experimental conditions: CaM concentrations were 1.2 μM for PM-CaM and in the case of all target peptides, except CaMKII20, the peptide concentration was 3.6 μM. The concentration of CaMKII20 was 1.7 μM. The medium contained 0.1 M HEPES (pH 7.5), 0.1 M KCl, 1 mM $MgCl_2$, and 0.1 mM $CaCl_2$. The temperature was 25 °C.

Overall Rotational Dynamics of CaM. The FRET measurements already discussed (see above) suggest that the two opposing globular domains in PM-CaM move into closer juxtaposition upon binding target peptides with a corresponding reduction in their associated conformational heterogeneity (Table 4). However, variations in the lifetime, solvent accessibility, and rotational dynamics associated with PM-CaM bound to the six target peptides used in these experiments suggest that there are differences in the tertiary structure of CaM bound to each of the six different target peptides. In order to further assess possible differences in the conformation of CaM bound to target peptides we have measured the global rotational motion of PM-CaM associated with target peptides, which provides information relating to the hydrodynamic properties of CaM when bound to target peptides. Using this information we are able to assess the overall dimensions of CaM, as described in Experimental Procedures. As discussed previously, calcium-saturated CaM is a nonspherical molecule with a correlation time (ϕ_2) of 10.9 ± 0.7 ns that is sensitive to rotational motion along the long axis of CaM (Yao et al., 1994). Upon association with each of the six target peptides, we observe no significant change in the rate of overall rotational motion of the CaM-peptide complex relative to calcium-saturated CaM. Since the CaM−peptide complex has a larger hydrated volume than calcium-saturated CaM, the similar rotational correlation times observed for CaM subsequent to peptide binding indicate that the overall dimensions along the long axis of PM-CaM become smaller. The observed average correlation time for CaM bound to each of the six target peptides (ϕ_2 = 10.6 ± 0.4 ns) is consistent with an prolate ellipsoid with an axial ratio of 2.3 (see eqs 12−15 in Experimental Procedures). The latter result is consistent with both the FRET data (which indicates that the two globular domains of CaM become spatially closer subsequent to peptide binding; see above) and the crystal structures of CaM bound to either RS20 or CaMKII20 which suggest that the overall dimensions of CaM bound to these target peptides can be approximated as an ellipsoid with an axial ratio of about 2 (Meador et al., 1992, 1993). The similar rotational correlation times observed for CaM bound to all six peptides indicate that the overall dimensions of CaM complexed to each of the six target peptides are virtually identical, consistent with a similar binding mechanism in which the two opposing globular domains of CaM bind to the amphipathic target peptides in an analogous manner.

The similar rotational correlation times (i.e., ϕ_2) associated with the hydrodynamic properties of the complex between CaM and each of the six target peptides (see Table 5) indicate that the two globular domains of CaM bind each of the six target peptides in a similar manner so as to maintain the overall dimensions of the complex between CaM and target peptides. An upper limit can be calculated with respect to the possible spatial heterogeneity between the opposing globular domains in CaM that are consistent with the observed uncertainties in the measured rotational correlation times relating to the hydrodynamic properties of CaM:peptide complex. If it is assumed that all CaM:peptide complexes can be modeled as prolate ellipses (see Experimental Procedures), then it can be calculated that a 4 Å relative displacement of one of the globular domains of CaM along the length of the target peptide (assuming no change in hydrated volume) would result in an increase in the rotational correlation time of about 0.5 ns. The observed correlation times are therefore consistent with the observed spatial heterogeneity between the opposing globular domains in CaM bound to the six target peptides used in this study that we observe using FRET as well as the 5 Å variation observed in the maximal dimension of CaM bound to analogous target peptides observed using small-angle X-ray scattering [reviewed by Trewhella (1992)].

DISCUSSION

In order to assess mechanistic features relating to the ability of CaM to productively associate with the autoinhibitory domains of a range of different target proteins which possess little sequence homology to one another, we have used frequency-domain fluorescence spectroscopy to measure the structural properties of CaM bound to six target peptides

with variable primary sequences. We observe similar decreases in the average fluorescence lifetime ($\bar{\tau}$) and similar increases in the solvent accessibility of PM bound at Cys_{27} in calcium binding loop I in the amino terminal domain of CaM upon association with each of the six target peptides, which approach values associated with the free probe in solution (Table 3). Likewise, we observe an analogous spatial separation between PM located at Cys_{27} in calcium binding loop I and nitrotyrosine$_{139}$ located in calcium binding loop IV for CaM bound to all six peptides (Table 4, Figure 5). This indicates that CaM undergoes comparable structural changes upon association with each of the six target proteins. However, there are significant differences in the observed lifetime, solvent accessibility, correlation time associated the segmental rotational motion of PM-CaM, and in the spatial separation between the opposing globular domains in CaM upon association with the individual target peptides, which indicates that the tertiary structure of CaM bound to target peptides is variable. The correlation times associated with the overall hydrodynamic properties of CaM complexed with all six peptides are nearly identical ($\phi_2 \approx 10.6 \pm 0.4$ ns; Table 5), and are consistent with the overall structure of CaM complexed with either CaMKII, RS20, or M13 which can be approximated as an ellipsoid with an axial ratio of approximately two (i.e., overall dimensions of 50 × 30 × 25 Å; Meador et al., 1993), as described in Experimental Procedures. These results are indicative of a common binding mechanism between CaM and each of the six target peptides, and are compatible with previous models that suggest variations in the amino acid side chains that form the peptide binding site on CaM are sufficiently flexible to allow CaM to associate with the variable sequences found in the autoinhibitory domains of target proteins with high affinity (Meador et al., 1993; Afshar et al., 1994).

Relationships to Other Studies. CaM binding domains have been identified in a range of different target enzymes, and in general are amphipathic peptides that bind CaM with an affinity analogous to that observed using the native enzyme and contain about twenty amino acids that adopt α-helical structures subsequent to the association with CaM [reviewed by Crivici and Ikura (1995)]. Small-angle X-ray scattering measurements have demonstrated that in general the complex formed between CaM and target peptides that adopt α-helical structures (including similar peptides to those used in this study that are homologous to the autoinhibitory domains of myosin light chain kinase, glycogen phosphorylase kinase, plasma membrane Ca-ATPase, and melittin) give similar overall structural parameters to that observed in the CaM:peptide complexes with M13, RS20, and CaMKII where high resolution structural information is available [reviewed by Trewhella (1992)]. However, in general agreement with the results presented in this study a small variation (~5 Å) in the maximal dimensions of the complex between CaM and target peptides was observed, consistent with the suggestion that there is some plasticity with respect to the binding mechanism between CaM and target peptides (Meador et al., 1993; Afshar et al., 1994).

Conclusions and Future Directions. We report that while the basic mechanisms of association between CaM and target peptides that are homologous to the autoinhibitory domains of CaM-regulated proteins are similar, that there are substantial variations in both the local environment within calcium binding loop I and in the spatial arrangement associated with the two opposing globular domains in CaM bound to target peptides. These results are consistent with a role for the central helix in permitting the two opposing globular domains of CaM to associate with variable target sequences in a conformation that maximizes both electrostatic and van der Waals interactions, and emphasizes the plasticity of CaM's structure in permitting a maximal binding interaction between variable target sequences. Future studies will emphasize (i) the possible regulation of CaM's functional properties by cellular signaling mechanisms involving both phosphorylation and oxidative modification at defined sites on CaM and (ii) the need to assess the structure of CaM-binding domains of target proteins and how their structure is modified upon CaM association.

ACKNOWLEDGMENT

We are grateful for the many helpful discussions provided by Diana Bigelow and J. David Johnson. We thank J. David Johnson for providing RS20, F52, and melittin. We thank Robert Steiner for providing PHK5.

REFERENCES

Afshar, M.; Caves, L. S. D., Guimard, L., Hubbard, R. E., Calas, B., Grassy, G., & Haiech, J. (1994) *J. Mol. Biol. 244*, 554−571.
Babu, Y. S., Sack, J., Greenough, T. J., Bugg, C. E., Means, A. R., & Cook, W. J. (1985) *Nature 315*, 37−40.
Babu, Y. S., Bugg, C. E., & Cook, W. J. (1988) *J. Mol. Biol. 204*, 191−204.
Bajzer, Z., & Prendergast, F. G. (1993) *Biophys. J. 67*, 2313−2323.
Barbato, G., Ikura, M., Kay, L., Pastor, R. W., & Bax, A. (1992) *Biochemistry 31*, 5269−5278.
Beechem, J. M., & Haas, E. (1989) *Biophys. J. 55*, 1225−1236.
Beechem, J. M., Gratton, E., Ameloot, M., Knutson, J. R., & Brand, L. (1991) in *Topics in Fluorescence Spectroscopy* (Lakowicz, J. R., Ed.) pp 241−305, Plenum Press, New York.
Bevington, P. R. (1969) *Data Reduction and Error Analysis for the Physical Sciences*, McGraw-Hill, New York.
Blackshear, P. J., Verghese, G. M., Johnson, J. D., Haupt, D. M., & Stumpo, D. J. (1982) *J. Biol. Chem. 257*, 13540−13546.
Blumenthal, D. K., & Krebs, E. G. (1988) *Molecular Aspects of Cellular Regulation* (Cohen, P., & Klee, C. B., Eds.) Vol. 5, pp 341−356, Elsevier, Amsterdam, The Netherlands.
Buckler, D. R., Haas, E., & Scheraga, H. A. (1995) *Biochemistry 34*, 15965−15978.
Cantor, C. R., & Schimmel, P. R. (1980) *Biophysical Chemistry*, Vol. 2, W. H. Freeman and Company, San Francisco, CA.
Chapman, E. R., Alexander, K., Vorherr, T., Carafoli, E., & Storm, D. R. (1992) *Biochemistry 31*, 12819−12825.
Chattopadhyaya, R., Meador, W. E., Means, A. R., & Quiocho, F. A. (1992) *J. Mol. Biol. 228*, 1177−1192.
Cheung, H. C. (1991) in *Topics in Fluorescence Spectroscopy* (Lakowicz, J. R., Ed.) Vol. 2, pp 128−176, Plenum Press, New York.
Crivici, A., & Ikura, M. (1995) *Annu. Rev. Biophys. Biomol. Struct. 24*, 85−116.
Dasgupta, M., Honeycutt, T., & Blumenthal, D. K. (1989) *J. Biol. Chem. 264*, 17156−17163.
Erickson-Vitanen, S., & DeGrado, W. (1987) *Methods Enzymol. 139*, 455−478.
Fairclough, R. H., & Cantor, C. R. (1978) *Methods Enzymol. 48*, 347−379.
Garcia de la Torr, J., & Bloomfield, V. (1981) *Q. Rev. Biophys. 14*, 81−139.
Graff, J. M., Young, T. N., Johnson, J. D., & Blackshear, P. J. (1989) *J. Biol. Chem. 264*, 21818−21823.
Gratton, E., & Limkeman, M. (1983) *Biophys. J. 44*, 315−324.
Haas, E., Katchalski-Katzir, E., & Steinberg, I. (1978) *Biochemistry 17*, 5064−5070.

Hahn, L. H. E., & Hammes, G. G. (1978) *Biochemistry 17*, 2433−2429.
Ikura, M., Clore, G. M., Gronenborn, A. M., Zhu, G., Klee, C. B., & Bax, A. (1992) *Science 256*, 632−638.
James, P., Vorherr, T., & Carafoli, E. (1995) *Trends Biochem. Sci. 20*, 38−42.
Johnson, M. L., & Faunt, L. M. (1992) *Methods Enzymol. 210*, 1−37.
Juminaga, D., Albaugh, S. H., & Steiner, R. F. (1994) *J. Biol. Chem. 269*, 1660−1667.
Kataoka, M., Head, J. F., Voherr, T., Krebs, J., & Carafoli, E. (1991) *Biochemistry 30*, 6247−6251.
Kemp, B. E., Pearson, R. B., Guerriero, V., Bagchi, I. C., & Means, A. R. (1987) *J. Biol. Chem. 262*, 2542−2548.
Kilhoffer, M.-C., Kubina, M., Travers, F., & Haiech, J. (1992) *Biochemistry 31*, 8098−8106.
Klee, C. B., Crouch, T. H., & Richman, P. G. (1980) *Annu. Rev. Biochem. 49*, 489−515.
Kretsinger, R. H., & Nockolds, C. E. (1973) *J. Biol. Chem. 248*, 3313−3326.
Lakowicz, J. R. (1983) *Principles of Fluorescence Spectroscopy*, Plenum Publishing Corp., New York.
Lakowicz, J. R., & Gryczynski, I. (1991) *Topics in Fluorescence Spectroscopy*, Plenum Publishing Corp., New York.
Lakowicz, J. R., Gryczynski, I., Cheung, H. C., Wang, C., Johnson, M. L., & Joshi, N. (1988) *Biochemistry 27*, 9149−9160.
Lehrer, S. S., & Leavis, P. C. (1978) *Methods Enzymol. 49*, 222−236.
Leudtke, R., Owen, C. S., Vanderkooi, J. M., & Karush, F. (1981) *Biochemistry 20*, 2927−2936.
Maulet, Y., & Cox, J. A. (1983) *Biochemistry 22*, 5680−5686.
Meador, W. E., Means, A. R., & Quiocho, F. A. (1992) *Science 257*, 1251−1255.
Meador, W. E., Means, A. R., & Quiocho, F. A. (1993) *Science 262*, 1718−1721.
O'Neil, K. T., & Degrado, W. F. (1990) *Trends Biochem. Sci. 15*, 59−64.
Payne, M. E., Fong, Y. L., Ono, T., Colbran, R. J., Kemp, B. E., Soderling, T. R., & Means, A. R. (1988) *J. Biol. Chem. 263*, 7190−7195.
Pedigo, S., & Shea, M. A. (1995) *Biochemistry 34*, 1179−1196.
Richman, P. G., & Klee, C. B. (1978) *Biochemistry 17*, 928−935.
Royer, C. A. (1993) *Biophys. J. 65*, 9−10.
Schöneich, Ch., Hühmer, A. F. R., Rabel, S. R., Stobaugh, J. F., Jois, S. D. S., Larive, C. K., Siahaan, T. J., Squier, T. C., Bigelow, D. J., & Williams, T. D. (1995) *Anal. Chem. 67*, 155R−181R.
Scott, T. G., Spencer, R. D., Leonard, N. G., & Weber, G. (1970) *J. Am. Chem. Soc. 92*, 687−695.
Seeholzer, S. H., Cohn, M., Putkey, J. A., Means, A. R., & Crespi, H. L. (1986) *Proc. Natl. Acad. Sci. U.S.A. 83*, 3634−3638.
Small, E. W., & Anderson, S. R. (1988) *Biochemistry 27*, 419−428.
Steiner, R. F. (1991) in *Topics in Fluorescence Spectroscopy* (Lakowicz, J. R., Ed.) Vol. 2, pp 1−52, Plenum Press, New York.
Strasburg, G. M., Hogan, M., Birmarchu, W., Thomas, D. D., & Louis, C. F. (1988) *J. Biol. Chem. 263*, 542−548.
Stryer, L. (1978) *Annu. Rev. Biochem. 47*, 819−846.
Tjandra, N., Kuboniwa, H., Ren, H., & Bax, A. (1995) *Eur. J. Biochem. 230*, 1014−1024.
Toda, H., Yazawa, M., Sakiyama, F., & Yagi, K. (1985) *J. Biochem. 98*, 833−842.
Török, K., Lane, A. N., Martin, S. R., Janot, J.-M., & Bayley, P. M. (1992) *Biochemistry 31*, 3452−3462.
Trewhella, J. (1992) *Cell Calcium 13*, 377−390.
Weber, G. (1981) *J. Phys. Chem. 85*, 949−953.
Yao, Y., Schöneich, C., & Squier, T. C. (1994) *Biochemistry 33*, 7797−7810.

BI960229K